

Molecular BioSystems

Accepted Manuscript



This is an *Accepted Manuscript*, which has been through the Royal Society of Chemistry peer review process and has been accepted for publication.

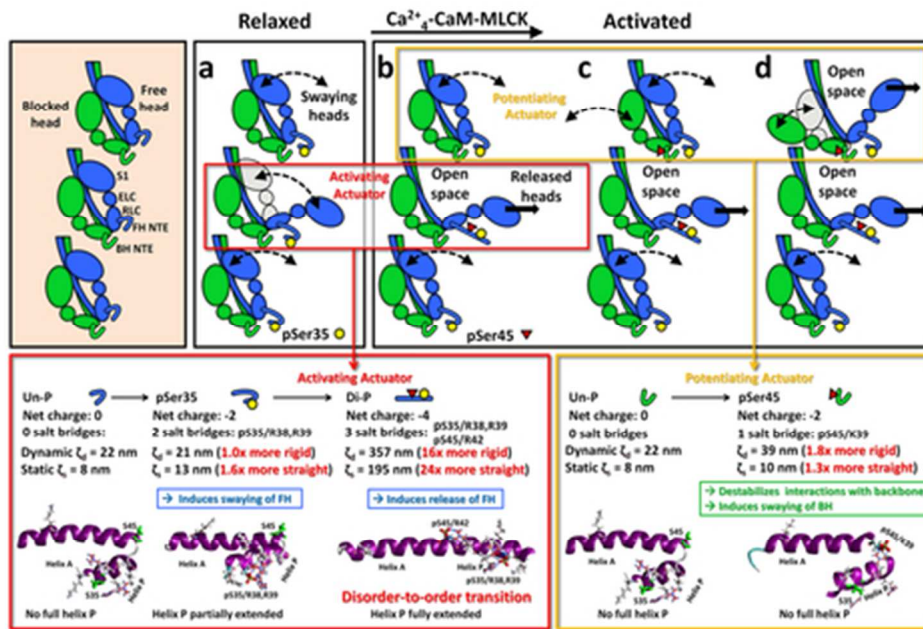
Accepted Manuscripts are published online shortly after acceptance, before technical editing, formatting and proof reading. Using this free service, authors can make their results available to the community, in citable form, before we publish the edited article. We will replace this *Accepted Manuscript* with the edited and formatted *Advance Article* as soon as it is available.

You can find more information about *Accepted Manuscripts* in the [Information for Authors](#).

Please note that technical editing may introduce minor changes to the text and/or graphics, which may alter content. The journal's standard [Terms & Conditions](#) and the [Ethical guidelines](#) still apply. In no event shall the Royal Society of Chemistry be held responsible for any errors or omissions in this *Accepted Manuscript* or any consequences arising from the use of any information it contains.



www.rsc.org/molecularbiosystems



Tarantula thick filament activation stiffens myosin regulatory light chain N-terminal extension by sequential phosphorylation hindering free head docking back
40x27mm (300 x 300 DPI)

Cite this: DOI: 10.1039/c0xx00000x

www.rsc.org/xxxxxx

PAPER

Tarantula Myosin Free Head Regulatory Light Chain Phosphorylation Stiffens N-terminal Extension Releasing it and Blocking its Docking Back

Lorenzo Alamo^a, Xiaochuan (Edward) Li^b, L. Michel Espinoza-Fonseca^c, Antonio Pinto^a, David D. Thomas^c, William Lehman^b, and Raúl Padrón^{a*}

^aCentro de Biología Estructural, Instituto Venezolano de Investigaciones Científicas (IVIC), Apdo. 20632, Caracas 1020^a, Venezuela.

^bDepartment of Physiology and Biophysics, Boston University School, 72 East Concord Street, Boston, MA 02118, USA

^cDepartment of Biochemistry, Molecular Biology and Biophysics, University of Minnesota, Minneapolis, Minnesota 55455, USA.

¹⁰*Corresponding author: Raúl Padrón (raul.padron@gmail.com, fax: +58 212 504 1444, phone +58 212 504 1098)

Received (in XXX, XXX) Xth XXXXXXXXXX 20XX, Accepted Xth XXXXXXXXXX 20XX

DOI: 10.1039/b000000x

Molecular dynamics simulations of smooth and striated muscle myosin regulatory light chain (RLC) N-terminal extension (NTE) showed that diphosphorylation induces a disorder-to-order transition. Our goal here was to further explore the effects of mono- and diphosphorylation on the straightening and rigidification of the tarantula myosin RLC NTE. For that we used MD simulations followed by persistence length analysis to explore the consequences of secondary and tertiary structure changes occurring on RLC NTE following phosphorylation. Static and dynamic persistence lengths analysis of tarantula RLC NTE peptides suggest that diphosphorylation produces an important 24-fold straightening and a 16-fold rigidification of the RLC NTE, while monophosphorylation has a less profound effect. This new information on myosin structural mechanics, not fully revealed by previous EM and MD studies, add support to a cooperative phosphorylation-dependent activation mechanism as proposed for the tarantula thick filament. Our results suggest that the RLC NTE straightening and rigidification after Ser45 phosphorylation leads to a release of the constitutively Ser35 monophosphorylated free head swaying away from the thick filament shaft in the relaxed state. This is so because the stiffened diphosphorylated RLC NTE would hinder the docking back of the free head after swaying away, becoming released and mobile and unable to recover its original interacting position on activation.

Introduction

Muscle contraction is controlled by Ca²⁺ concentration through molecular switches located in the thin and thick filaments.¹ In the latter, Ca²⁺ control occurs directly by Ca²⁺ binding to the myosin essential light chains² or indirectly by Ca²⁺-binding to calmodulin, followed by activation of the myosin light chain kinase (MLCK) which phosphorylates the myosin regulatory light chain (RLC). In vertebrate smooth muscle the regulatory mechanism is a MLCK-based phosphorylation³ while in arthropod (*Limulus*, tarantula, scorpion)⁴⁻⁶ and vertebrate striated muscles³ such phosphorylation occurs in addition to troponin-tropomyosin (TN/TM) actin-linked regulation. The structural basis of tarantula striated muscle regulation has been widely studied as a model system, because of the highly ordered thick filaments assembly in these muscles.^{5,7-12}

Vertebrate smooth and invertebrate striated muscle myosin

RLC contains phosphorylatable serines on its N-terminal extension (NTE) (Fig. 1Aa,b). Phosphorylation at serine 19 in smooth muscles has been comprehensively studied (Fig. 1Aa). Electronic paramagnetic resonance (EPR) spectroscopy showed that smooth muscle NTE becomes more helically ordered and solvent accessible after phosphorylation.¹³ Molecular dynamics (MD) simulations of isolated smooth muscle NTE further showed that (a) this domain undergoes a disorder-to-order transition upon phosphorylation¹⁴ and (b) dephosphorylation acts as a molecular switch to reverse the phosphorylation-induced conformational transition.¹⁴ In fact, time-resolved fluorescence resonance energy transfer experiments and MD simulations revealed the presence of two RLC structural states, where phosphorylation switches the system from a closed state to a more dynamic helically ordered open structural state.^{15,16}

In tarantula striated muscle, with a relatively large 52 amino acid (aa) NTE (Fig. 1Ab), MD on the NTE revealed a similar disorder-to-order transition as in smooth muscle occurring only

after Ser45 diphosphorylation of previously Ser35 monophosphorylated free heads. Ser35 monophosphorylation alone, however induced only a partial disorder-to-order transition.¹⁷ These MD simulations suggest that a disorder-to-order transition similar to that of smooth muscle is conserved. In contrast, no such transition was seen on MD trajectories upon Ser45 monophosphorylation of free or blocked head RLC NTEs. This suggested that the release of force-potentiating heads would be controlled by a different mechanism, -not based on a disorder-to-order transition- but instead probably electrostatic in nature, inducing a flexibilization of the myosin regulatory domain.¹⁷ It was concluded that tarantula thick filament activation, is controlled through a helix-P disorder-to-order transition promoted by sequential Ser35 and Ser45 phosphorylation. Force potentiation, on the other hand, is controlled through the eventual flexibilization of the regulatory domain by phosphorylation at Ser 45. Molecular actuators, located in the PKC and MLCK consensus sequences of the RLC NTE helix-P (P_{PKC} and P_{MLCK} , Fig.1B), allow the sequential release of the free and blocked heads as proposed by the cooperative phosphorylation mechanism for tarantula striated muscle activation and potentiation (Fig. 4).^{11,12}

MD simulations provide structural information in atomic detail that cannot be easily accessed experimentally; therefore, the conformational assemblage obtained from MD simulations can be used –as we propose here- to measure various properties such as the flexibility and curvature of a molecule. Hence, we used the structural assemblages to calculate the phosphorylation-induced flexural rigidity changes on the large 5.6 kDa tarantula RLC NTE. The flexibility of coiled-coil α -helical proteins has been studied by viscoelastic and capillary viscosity measurements.¹⁸ The curvature, flexibility and persistence length of the tropomyosin coiled coils has been studied extensively using this approach.¹⁹⁻²¹ Here, we devised a method based on the analysis of the apparent, dynamic and static persistence lengths of NTE as it evolves during MD simulations from an initially fully straight NTE (Fig. 1B). Our goal here is to further explore the effects of mono- and diphosphorylation on the flexural rigidity of tarantula myosin RLC N-terminal extension by assessing its straightening and rigidification through the calculated NTE persistence length and compare to the unphosphorylated RLC NTE, in order to understand how NTE phosphorylation controls the sequential release of the free and blocked myosin heads following muscle activation.

Methods

MD systems setup

To investigate the effect on the RLC NTE straightness and rigidity in different phosphorylation states we did a flexural rigidity analysis starting from a theoretical fully straightened RLC NTE (Fig. 1B). The 66-aa fully straightened starting structure, formed by the 52-aa NTE domain plus the adjacent 14-aa from helix A (Fig. 2A left) was modelled as an ideal α -helix using Swiss PDB Viewer.²² This structure was then used for the 4 peptides investigated, viz. unphosphorylated (un-P), two monophosphorylated (mono-P) on Ser35 (pSer35) or Ser45 (pSer45), and one diphosphorylated (di-P). We followed methods

described in.¹⁴ Peptides were capped with an acetyl group and a N-methylamide at the N- and C-terminus respectively, and embedded in a $100 \text{ \AA} \times 100 \text{ \AA} \times 100 \text{ \AA}$ TIP3P model water box. To mimic the physiological-like ionic strength we added 150 mM NaCl. The CHARMM22 all-atom force field was employed.²³

Molecular dynamics simulation protocol

MD simulations were performed using NAMD version 2.5.^{14,24} Periodic boundary conditions,²⁵ particle mesh Ewald method,^{26,27} a nonbonded cutoff of 9 \AA and a 2 fs time step were used. The standard physiological conditions were maintained with a Langevin barostat (1 atm) and thermostat (310 K). Energy minimizations were done with initial 1000 steps set by a conjugate-gradient algorithm with restraints to the protein backbone, followed by additional 1000 steps, but without restraints. Temperature was increased for 20 ps, and then equilibrated for 60 ps with lower restraints, finishing at 310 K with no restraints. Simulations of 66-aa peptides were done on a Beowulf cluster of 32 dual-core Opteron processors. Due to the long duration of the MD simulations (hundreds of ns), only one simulation was made for each phosphorylated state.

Analysis, visualization and rendering of peptides

Molecular graphics images for the Fig. 1 were produced using the UCSF Chimera package.²⁸ The analysis, visualization and rendering of peptides were performed with Visual Molecular Dynamics (VMD).²⁹ Two VMD plugins were used: the RMSD Trajectory Tool at 0.2 steps/ns, to calculate the root mean square deviation between all peptides atoms and to estimate their structural stability; and STRIDE,³⁰ to analyze the peptides secondary structure evolution.

Flexural rigidity analysis

Persistence length (ξ), a mechanical quantity, is used to describe the “stiffness” or “flexibility” of a rod, which can be calculated as

$$\xi = -s / \ln \langle \cos(\theta) \rangle \quad (1)$$

where θ is the bending angle and s the contour length of the rod, obtained by measuring the snapshots in the trajectory, which are generally nearly straight (Movies S7-8 in Supporting Material). ξ is the length over which the tangent vector of the rod bends 68.4° (when denominator term $\ln \langle \cos(\theta) \rangle = -1$) on average while one end is fixed: i.e. a stiff rod has a larger ξ (smaller bending angle θ) while a flexible one has a shorter ξ (larger bending angle θ). A coiled-coil α -helical protein, such as tropomyosin, can be described as a semi flexible rod with ξ values of $130 \pm 40 \text{ nm}$.¹⁸ In general, persistence length describes both how curved and flexible a rod is. The assumption here is that in a force-free environment, if a rod is straight on average, then persistence length (ξ) is a correct metric to describe the rod flexibility. However, if the average shape of a rod adopts a curved shape, then the persistence length (ξ) is not sufficient to describe the rod flexibility. Trifonov et al.^{31,32} suggested that a “static” and “dynamic” persistence length can be distinguished using the equation:

$$1/\xi_a = 1/\xi_d + 1/\xi_s \quad (2)$$

where ξ_a is the *apparent persistence length* (determined by

equation 1), ξ_d is the *dynamic persistence length* (related with thermal fluctuation) and ξ_s is the *static persistence length* (related with its average shape). Li et al.^{20,21} pointed out that δ , the angular deviation from the rod average position, can be used to calculate the ξ_d and thus to describe the true rigidity of the rod. They^{20,21} proposed the dynamic persistence length ($\xi_d = -s / \ln \langle \cos(\delta) \rangle$) to describe the flexibility/rigidity of a curved rod. For instance, tropomyosin has an apparent ξ_a of 104 nm but a dynamic ξ_d of 423 nm.²⁰ In other words ξ_s describes the curvature or bending curvature of the molecule, whereas ξ_d describes the rigidity of the molecule. Here we used this methodology to calculate ξ_a and ξ_d from MD simulations of fully extended NTEs to investigate its curvature/straightness and flexibility/rigidity.

To quantify the bending at both phosphorylation sites, we defined two bending angles (θ_1 and θ_2) as formed by three vectors: *vector 1* (helix A), *vector 2* (P_{MLCK}, part of the MLCK phosphorylation site on helix P) and *vector 3* (P_{PKC}, part of the PKC phosphorylation site on helix P) (Fig. 1Ac). The angles θ_1 and θ_2 are a simple measure of the change in orientation of the helical

axis as one proceeds (from C-terminal to N-terminal) i.e. from helix A to the first segment of helix P (P_{MLCK}) to the second segment of helix P (P_{PKC}). In other words, the angles θ_1 and θ_2 reflect directional changes on the respective phosphorylation target regions Ser45 (P_{MLCK}) or Ser35 (P_{PKC}) of helix P. Because it requires 3.6 residues for a complete α -helix turn, we calculated the centre of backbone atoms over at least four or more residues. Therefore the three vectors were defined as the centres of sequences EFKEAF to TQHQQVQ; NVFAMF to KRRAQR; and QKRRRAQ to PAPKPP (Fig. 1Ab). The angles between vector 2 (MLCK target) and 3 (PKC target) is θ_1 and between vector 1 (helix A) and vector 2 (MLCK target) is θ_2 (Fig. 1Ac). Because as described above angles θ_1 and θ_2 are defined in different regions along the rod we defined angle θ as the average of θ_1 and θ_2 , and used it to capture the average bending along these regions (Fig. 1Ac). Thus the static persistence length (ξ_s), obtained from equation (2), gives a measure of the straightness of the NTE in the helices A and P region. The results are listed in Table 1 and Supplementary Table 1.

Table 1 Comparison between the un-, mono- and di-P tarantula RLC NTE peptides charge, conformation, secondary structure and flexural rigidity

Phosphorylation state	Un-P	Mono-P Constitutive pSer35	Mono-P Activating pSer45	Di-P pSer35 and pSer45
NTE net charge	0	-2	-2	-4
MD from a straight NTE Helices P and A Helix to turn/coil HCH folding Salt bridges	Continuous up to Ser45 P31-K32 S43-G44 No salt bridges	Continuous up to Ser45 P31-K32 G44 pS35/R38,R39	Continuous up to Ser45 No S43 pS45/R39	Continuous up to Pro31 No No pS35/R38,R39 pS45/R42
Persistence Length of NTE				
Angle $\langle \theta_1 \rangle$ degrees	50.4	43.6	61.2	8.8
Angle $\langle \theta_2 \rangle$ degrees	53.2	40.6	33.8	15.0
Apparent ξ_a (nm) ^a	6 [1.0] ^c	8 [1.3] ^c	8 [1.3] ^c	126 [21.0] ^c
Dynamic ξ_d (nm) ^a	22 [1.0] ^c	21 [0.95] ^c	39 [1.8] ^c	357 [16.2] ^c
Static ξ_s (nm) ^b	8 [1.0] ^c	13 [1.6] ^c	10 [1.3] ^c	195 [24.4] ^c

^a Calculated from angles $\langle \theta_1 \rangle$ and $\langle \theta_2 \rangle$.

^b Calculated using $1/\xi_s = 1/\xi_a - 1/\xi_d$.

^c The values relative to un-P are shown in brackets.

When the bending angles (θ_1 and θ_2) at phosphorylation sites are used as the metrics to describe the extent of structural changes, the variance of these bending angles should give us an indication how easy/hard the structure changes its rigidity. Zuccheri et al.³³ used the variance of curvature angle to quantify the flexibility of DNA. We decided to use the variance of the average bending angle (θ) to quantify the rigidity of the NTE in the helices A and P region, which in turn is related to the dynamic persistence length (ξ_d) by the relationship:

$$\xi_d \cong \frac{2s}{\langle \theta^2 \rangle - \langle \theta \rangle^2} \quad (3)$$

where s is the contour length of the distance along the centres of residues 30 (PPAP) to 64 (AFQL) of the di-P and the denominator is the variance of average bending angle θ . We choose $\langle \theta^2 \rangle - \langle \theta \rangle^2 = \text{variance}(\theta) = \text{the maximum value of (variance}(\theta_1), \text{variance}(\theta_2))$ to capture the largest bending events (calculations shown in Supplementary Table 1).

To roughly have the same data points in the ξ calculation as in the MD simulations (Fig. 3, bottom panel), the sampling

frequency was set as 1/5 from the un-P or di-P trajectories files (0.3 steps/ns), and 1/10 from mono-P trajectory files (0.8 steps/ns for pSer45 and 0.5 steps/ns for pSer35).

Results

We investigated the effect of phosphorylation on the curvature and flexibility of the RLC NTE by analysing the flexural rigidity of these NTEs under different conditions (Fig. 2, 3).

RLC NTEs MD simulations

Unphosphorylated NTEs: The unphosphorylated 52-aa NTE stabilized in ~ 100 ns, as revealed by smaller deviations in the RMSD evolution plot (Fig. 3A, centre panel, black arrow), but at a much slower rate than the shorter 25-aa RLC NTE from chicken gizzard.¹⁴ This slower stabilization time is probably due to the inertial mass of helix L and the larger peptide structure (25 vs. 66 aa) and a Pro/Ala linker. The conformation of the unphosphorylated NTE stabilized at ~ 200 ns consists of three helical segments corresponding to helices A, P and L (Fig. 2A,

right), with $\langle\theta_1\rangle = 50.4^\circ$ and $\langle\theta_2\rangle = 53.2^\circ$ angles (Table 1). The helix P is bended onto helix A at Ser45 (Fig. 2A right); the evolution of this change showed a loss of α -helical structure at Pro31-Lys32 extending the linker (Fig. 3A, top panel, red arrowhead) and a bending at Ser42-Gly44, as a helix-coil-helix (HCH) folding structure (black arrow, Fig. 3A, top panel) in ~80 ns, and no salt bridges were established (Fig. 3A top panel, Table 1, Movies S1-S2).

Ser45 monophosphorylated NTE: The Ser45 mono-P NTE stabilized even more slowly (~530 ns, Fig. 3B, middle panel, black arrow), also evolving (in ~600 ns) into a compact structure (Fig. 2B) induced by a bend at pSer45 with $\langle\theta_1\rangle = 61.2^\circ$ and $\langle\theta_2\rangle = 33.8^\circ$ angles. The evolution of this change (Fig. 3B, top panel) showed a HCH folding structure at Ser43-Gly44 in ~480 ns (Fig. 3B, top panel, black arrow), and a salt bridge at pSer45/Arg39 (Fig. 2B yellow arrow, 3B, Movies S3-S4).

Ser35 monophosphorylated NTE: The Ser35 monophosphorylated NTE stabilized after ~280 ns (Fig. 3C, middle panel, black arrow) and evolved into a compact structure in ~350 ns (Fig. 3C) induced by a bend at Ser45, with angles $\langle\theta_1\rangle = 43.6^\circ$ and $\langle\theta_2\rangle = 40.6^\circ$. The evolution of the secondary structure (Fig. 3C top panel) showed a HCH folding structure of helix P in ~190 ns at Gly44 (Fig. 3C, top panel, black arrow), and that the linker extended the turn up to Lys32 (in ~270 ns) (Fig. 3C, top panel, red arrowhead), with dual salt bridges at pSer35/Arg38,Arg39 (Fig. 2C, yellow arrow, 3C, Movies S5-S6).

Ser35 and Ser45 diphosphorylated NTE: The diphosphorylated NTE stabilized very rapidly (only ~80 ns, Fig. 3D, middle panel, black arrow), and, in contrast to the un- and monophosphorylated NTEs, showed fully straightened helices P and A (Fig. 2D), with much smaller angles ($\langle\theta_1\rangle = 8.8^\circ$ and $\langle\theta_2\rangle = 15.0^\circ$). The evolution of the secondary structure (Fig. 3D, top panel) showed dual salt bridges at pSer35/Arg38,Arg39 and a salt bridge at pSer45/Arg42 (Fig. 2D, yellow arrows, Movies S7-S8). A similar straightening, due to a disorder-to-order transition, was found in the shorter 25-aa smooth muscle NTE when phosphorylated at Ser19.¹⁴

Helix L, connected to helix P by a flexible Pro/Ala linker (Fig. 1Ab,B), moved freely and ended up close to helix A (Fig. 2A-C, helix L shadowed); except for the diphosphorylated peptide (Fig. 2D, helix L shadowed), in which helix L established a weak interaction with helix P, and a pSer45/Lys15 salt bridge was established between helices L and P (Fig. 2D, blue arrow, Movies S7-S8).

Flexural rigidity of the RLC NTEs

Flexural rigidity analysis is shown in Fig. 3 (bottom panels) and Table 1. The results show that the flexural rigidity of tarantula RLC NTE large 5.6 kDa can be assessed, specifically by examining its straightness and rigidity using the approach proposed in this work. The proximity of helix P to helix A facilitates our persistence length analysis (ie. from a fully straightened NTE helix L, coil linker, helix P and helix A) because the θ_1 and θ_2 angles chosen for vectors 2 and 3 closely reflect the structural changes in critical different consensus sequences on key helices P_{PKC} and P_{MLCK} around the crucial Ser35 and Ser45 phosphorylatable residues (Fig. 1Ac).

The monophosphorylated NTE becomes straighter and more

rigid than the unphosphorylated NTE only when Ser45 is monophosphorylated: The ξ_s (13 nm) value for the Ser35

monophosphorylated NTE, implies an ~1.6-fold straightening over the $\xi_s = 8$ nm values for the unphosphorylated NTE (Table 1). The ξ_{ss} (10 nm) value for the Ser45 monophosphorylated NTE, implies a ~1.3-fold straightened over the $\xi_s = 8$ nm for the unphosphorylated NTE (Table 1). The changes in the ξ_s value suggests that the NTE is straightened after Ser35 or Ser45 monophosphorylation, while the ξ_d values (21 and 39 nm) suggest that only when Ser45 is monophosphorylated the NTE is more rigid (~1.8-fold) than the unphosphorylated NTE (22 nm) (Table 1). This could be related to the shapes of both free and blocked myosin heads RLC NTE regions observed on the intact frozen-hydrated thick filaments in 3D-maps.¹⁰ The straighter ~1.6-fold NTE could modify the flexibility of the regulatory domain of the constitutively Ser35 monophosphorylated free heads allowing them to sway away.^{11,12}

The diphosphorylated NTE is greatly straightened and rigidified: The ξ_s (195 nm) and ξ_d (357 nm) values of the diphosphorylated NTE (Table 1) implies it is greatly straightened (>24-fold) and rigidified (>16-fold) in comparison with the unphosphorylated NTE values of ξ_s (8 nm) and ξ_d (22 nm) (Table 1). We conclude that the disorder-to-helical-order transition that diphosphorylation produces, greatly straightens and rigidifies the NTE.

Discussion

Comparison with previous MD simulations of smooth and striated RLC NTEs

MD simulations of vertebrate smooth muscle 25-aa short NTE¹⁴ and tarantula striated muscle 52-aa long RLC NTE of¹⁷ have been previously performed, showing in both cases a disorder-to-order transition first proposed by Espinoza-Fonseca et al¹⁴ and suggesting that a generally conserved mechanism operates in smooth and striated muscle.

Vertebrate smooth muscle RLC NTE: MD simulations of isolated smooth muscle NTE showed that this domain undergoes a disorder-to-helical-order transition following a single phosphorylation. These smooth muscle NTE simulations were performed starting with fully extended and straight NTEs as done in the current work.

Tarantula striated muscle RLC NTE: In contrast to the present study, in¹⁷ the starting structures for the MD simulations considered the asymmetry of the myosin interacting-heads motif, especially in the RLC region.^{10,34} Therefore the initial structures used for the MD simulations were the ones representing the free and blocked heads as determined by the cryo-electron microscopy 3D-reconstruction of intact thick filaments deposited in the Protein Data Bank (PDB)³⁵ as 3DTP.¹⁰ We used here a synthetically elongated NTE¹⁴ to measure the NTE flexural rigidity, which would otherwise be impossible. The initial structures¹⁷ in relaxed state (PDB 3DTP),¹⁰ of both free and blocked heads were compact, and remained compact after 1,200 ns equilibration time. Then these stabilized conformations were used for the MD simulations of the monophosphorylated and diphosphorylated free and blocked head peptides. The monophosphorylated peptides evolved into compact structures as

well, except for the Ser35 monophosphorylated free head that exhibited a partial disorder-to-order transition; while the diphosphorylated peptide for the free head evolved to a fully straightened structure, exhibiting a disorder-to-order transition. In contrast,¹⁷ the artificial elongation of the NTE done here already introduced a partial increase on helicity of helix P, extending it along helix A. In our previous work¹⁷ we used initially stabilized compact structures. This allows for the formation of different salt bridges as the ones shown here: three salt bridges at the constitutively Ser35 monophosphorylated free head (pSer35/Arg38,Arg39, Arg42, vs. pSer35/Arg38,Arg39 here), one salt bridge in the Ser45 monophosphorylated blocked head (pSer45/Lys37 vs. pSer45/Arg39 here) and three salt bridges in the diphosphorylated free head (pSer35/Arg38,Arg39,Arg42 vs. pSer35/Arg38,Arg39 and pSer45/Arg42 detected here). The approach of using starting structures with compact conformations stabilized from the relaxed free and blocked head RLC NTE structures (PDB 3DTP)¹⁰ allowed the formation of crucial salt bridges present only in the constitutively Ser35 monophosphorylated free head RLC NTE, supporting its role as a swaying head.¹⁷ It is worth noting that both, the non straightened relaxed 3DTP NTE structures for the free and blocked heads¹⁷ and the completely different fully straightened NTE (Fig. 1B, 2A left) unphosphorylated and monophosphorylated (pSer35 or pSer45) evolved to similarly compact structures with helix-P folded over helix-A with a closer helix-L, suggesting that the conformational states shown in Fig. 2A,B,C are not metastable ones while diphosphorylation formed a stable extended A and P helices.

Previous studies in other systems reported similar calculations using much shorter trajectories³⁶ which have correctly predicted the physical properties of long helices consistent with small-angle x-ray scattering (SAXS) and single-molecule optical-trap analyses.

Implications of NTE flexural rigidity on tarantula thick filaments cooperative phosphorylation activation mechanism

Our MD simulations and flexural rigidity measurements provide a structural basis for the RLC phosphorylation, activation and potentiation model proposed for the tarantula thick filament (Fig 4).^{11,12,17} We analyze below the significance of these flexural rigidity changes in the context of the phosphorylation activation mechanism for the tarantula thick filament.^{11,12,17} The originally proposed mechanism¹¹ was based on our preliminary MD simulations performed only on tarantula diphosphorylated NTE, implying it would elongate and stiffen the NTE, as confirmed and extended by the MD results of¹⁷ and MD results presented here (Fig. 2D) as an important increase in the ξ_d and ξ_s persistence length values (Fig. 3D, Table 1) implies an important increase in NTE straightening and rigidity.

In this mechanism (Fig. 4), diphosphorylation of the constitutively Ser35 monophosphorylated free swaying heads induces a disorder-to-order transition which fully elongates the helix P along the helix A.¹⁷ The increase of ξ_d and ξ_s (Table 1) are in agreement with NTE elongation suggesting that the di-P NTE straightens and rigidifies it substantially. This elongation modifies the free head regulatory domain hindering the docking back of this head after it swaying away, as it cannot recover its

original interacting position. This hinders the S2 intramolecular interaction,¹⁰ so the free head becomes released and mobile as swinging heads in the crossbridge cycle.³⁷

In contrast, the Ser45 monophosphorylation of the blocked head NTE (Fig. 4c top) does not produce any major conformational change but increases the NTE net negative charge establishing the salt bridge pSer45/Arg39 and inducing a ~1.8-fold increase in dynamics persistence length (ξ_d). These could weaken the electrostatic interaction of the NTE of the blocked head RLC with a loop on the motor domain of the neighbour free head. The concomitant increased rigidity turns the blocked head into a swaying head-hindering the docking back of its partner free head NTE, which is constitutively monophosphorylated on its Ser35. This in turn releases this partner free head which become mobile (Fig. 4d top).

The results shown in Fig. 2 and 3 support the proposal of¹⁷ that in tarantula, the sequential Ser35-Ser45 phosphorylation controls (via a helix-P disorder-to-order transition) the activation of thick filament as summarized in Fig. 4. Two molecular actuators, located in the helix P_{PKC} and P_{MILCK}, allow the sequential release of the free and blocked heads as proposed by the cooperative phosphorylation mechanism for activation and potentiation of tarantula striated muscle.^{11,12,17}

Implications for the phosphorylation-based activation mechanism

A mechanism for activation in striated muscle bipolar thick filaments, in which several helices of myosin interacting-heads motifs are established, should take into account the asymmetry of the phosphorylation domain of both the free and blocked heads, as well as the intermolecular interactions between myosin interacting-heads motifs along the helices. We take both requirements into consideration in the activation mechanism for tarantula striated muscle thick filaments as shown in Fig. 4.

Recently we showed that the structure of Schistosoma smooth muscle thick filaments³⁸ (Sulbarán et al. in preparation) is almost identical to the tarantula one.^{10,34} This similarity, together with the close similarity between the 52- and 56-aa long myosin RLC NTEs of tarantula striated and schistosoma smooth muscles¹⁰ suggests that the mechanism proposed in Fig. 4 could be used in striated and smooth muscle bipolar thick filaments. In contrast, the lack of knowledge of the structure of vertebrate smooth muscle side-polar thick filaments has hindered the proposal of a mechanism for activation in these filaments.

Nevertheless, several proposals have been advanced to explain the activation of isolated vertebrate smooth muscle myosin molecules, some involving the myosin RLC NTE.^{14,15,39,40} Earlier studies suggested that a salt-bridge formed between Arg16 and Ser19^{14,39} upon Ser19 phosphorylation produced a disorder-to-order transition.¹⁵ It was suggested that the RLC NTE phosphorylated domain was completely α -helical and an extension of the RLC helix-A.¹⁵

Lately an ELC role has been proposed for the activation of vertebrate smooth muscle myosin by RLC phosphorylation⁴¹ based on site directed mutagenesis results which suggest that interactions between the phosphorylated smooth muscle RLC NTE and helix-A of the ELC are required for phosphorylation to activate smooth muscle myosin. It is not clear how this model,

proposed for isolated vertebrate smooth muscle myosin interacting-heads motifs, could be extended to smooth muscle vertebrate side-polar thick filaments.

In contrast to the mechanism proposed for vertebrate smooth muscle myosin activation,⁴¹ the model we propose here for tarantula striated muscle is for the activation and potentiation of bipolar thick filaments (Fig. 4), and suggests that myosin RLC phosphorylation induces a disorder-to-order transition, as proposed for vertebrate smooth muscle,^{14,39} through the formation of three salt bridges and extending helix-P along the RLC helix-A only on the swaying free heads.¹⁵ In tarantula the RLC NTE is involved in the interaction with the neighbour free head along the helix on myosin interacting heads motifs¹⁰ possibly through the positively charged helix L. This suggests that -in tarantula- the phosphorylation mechanism of the free head is based on the disorder-to-order mechanism^{14,15,39,40} while the mechanism for the blocked head -in contrast- could involve the ELC without a complete disorder-to-order transition.⁴¹

Could this thick filament activation mechanism be extended to striated muscles of other species?

While the constitutive PKC-dependent Ser35 monophosphorylation in tarantula relaxed filaments is required for rapid response to Ca²⁺ activation, Ser45 mono- or diphosphorylation by MLCK is used to slowly potentiate contraction.¹¹ Our MD simulations results provide a structural basis for the RLC phosphorylation, activation and potentiation as proposed for the tarantula thick filament (Fig 4).^{11,12} Understanding more about this mechanism is important, as RLC phosphorylation was the first mechanism evolved to control striated, smooth and nonmuscle contraction.⁴² The required enzyme (MLCK) was identified as an earlier metazoan innovation, allowing Ca²⁺-control by phosphorylating RLC.⁴²⁻⁴⁴ All the required components (myosin, RLC, calmodulin, MLCK and MLCP) for this type of regulation scheme are present in all animals.⁴² Three prerequisites need to be fulfilled for this mechanism (Fig. 4) to operate in striated muscle: (1) the assembly of geometrically appropriate myosin interacting-heads motifs in thick filaments,^{10,34,45} (2) the presence of RLCs with NTEs exhibiting a pair of phosphorylatable serines, associated with two specific kinase/phosphatase pairs; and (3) the formation of specific PKC- and MLCK-formed salt bridges. We conclude (see Supplementary Discussion) that these requirements are fulfilled by arthropods and platyhelminthes, as they have thick filaments with 4 helices of myosin interacting-heads motifs, long NTEs and the required PKC and MLCK phosphorylatable serines.

Acknowledgements

We thank Dr. Gustavo Márquez for his help with the manuscript. Molecular graphics image (Fig. 1B) was produced using the UCSF Chimera package²⁸ from the Resource for Biocomputing, Visualization, and Informatics at the University of California, San Francisco (supported by NIH P41 RR-01081). Fig. 2-3 and Supplementary Movies S1-S8) were produced using the Visual Molecular Dynamics (VMD) program²⁹. Computational resources were also provided by the Boston University Scientific Computing and Visualization Group. This work was supported by

grants from the National Institutes of Health (AR32961 to D.D.T., HL86655 and HL36153 to W.L.), the American Heart Association (10POST4350076 to L.M.E.F.) and the Howard Hughes Medical Institute (HHMI, to R.P.).

Legends

Fig. 1 The NTEs of the smooth and tarantula myosin RLCs. (A) Sequence alignment of the NTEs of chicken smooth (a) and tarantula striated (b) muscles. Phosphorylatable serines are in yellow (Ser35) and red (Ser45). Helix L (yellow), coil Pro/Ala linker (orange), helix P formed by PCK (blue) and MLCK (green) target consensus sequences, adjacent to the EF helix A (purple, Gln53-Ile66).¹⁰ (c) Vectors and angles as defined for the flexural rigidity analysis (see Methods). (B) Straightened tarantula RLC fragment used as the starting structure for MD simulations and flexural rigidity analysis. The 52-aa NTE (formed by helix L, linker and helix P) is adjacent to the RLC helix A (purple). The helix L has 9 positively charged lysines, and is connected by a flexible linker to the helix P, with includes the PKC (P_{PKC}, blue) and MLCK (P_{MLCK}, green) consensus sequences with their phosphorylatable Ser35 and Ser45.

Fig. 2 Snapshots showing key structural features of trajectories. The starting structure was assumed to be a straight α -helix. This peptide was equilibrated for the un-P (shown on the left part of A), pSer45, pSer35 and di-P MD simulations. Final simulation states of the stabilized structures are shown on A-D. Helix P bends bent over helix A in A-C but stays straightened on D. There is a linker extension at Pro31-Lys32 becomes coil/turn in A and C but not in B and D. Helix P is always bend at Ser45 except in D, where helices P and A remain straight. No salt bridges are established in un-P state A. Salt bridges (yellow arrows) are established for the mono-P states: pSer35/Arg38,Arg39 in C or pSer45/Arg39 in B; and salt bridges pSer35/Arg38,Arg39, and pSer45/Arg42 in D. Helix L (shadowed) moves freely around the flexible linker in all conditions, interacting eventually with helix-A in A-C, but in di-P (D) inter-helix pSer45/Lys15 salt bridge between helix L and A is established (blue arrow).

Fig. 3 Top panels: Evolution of secondary structure of NTE helix P along their trajectories: un-P (A), Ser45 (B) or Ser35 (C) mono-P, and di-P (D). Snapshots illustrating the final key structural features are shown in Fig. 2. Helix to coil/turns: at Pro31-Lys32 (A,C) (red arrowheads). HCH: at Ser43-Gly44 (A, B) and Gly44 (C) (black arrows). Vertical axis: one-letter code aa number. Secondary structure key colours: α -helix (pink), turn (cyan), coil (white). Centre panel: root mean square deviation (RMSD) of the NTE peptides trajectories of each phosphorylated state shown in Fig. 2. Arrows show that peptides stabilized after 100 (A), 530 (B), 300 (C) and 80 (D) ns. Bottom panel: Persistence length analysis ($|\theta|$ vs. time) of the NTEs. The angle $|\theta|$ captures the bending of the α -helix of the three vectors regions (Fig. 1Ac). The angle $|\theta|$ changed to $\sim 90^\circ$ for the un-P (A), to $\sim 80^\circ$ for Ser45 (B) or Ser35 (C) mono-P cases, and does not changed much ($\sim 10^\circ$) for the Di-P state (D). The result in (D) shows an important increase of straightening and rigidification (Table 1) only induced by diphosphorylation.

Fig. 4 The cooperative phosphorylation-controlled mechanism for recruiting active heads in tarantula thick filament activation.^{11,12,17} The three myosin interacting-heads motifs on the

left are shown along one thick filament helix with their entire RLC NTEs unphosphorylated (bare zone at the top). This mechanism shows how the Ser45 phosphorylation of the constitutive Ser35 monophosphorylated swaying free head NTE (b, centre IHM) hinders its docking back making it permanently mobile (b, arrow). Two *actuators* (red and yellow boxes) control the sequential release of myosin heads on tarantula thick filament activation.¹⁷ *Activating actuator* (red boxes): according to our MD simulations the activating actuator is based on a disorder-to-order transition of the RLC NTE, which induces its elongation in accordance with the increase of the static and dynamic persistence length ξ_s and ξ_d . This implies a substantial straightening and rigidification of the diphosphorylated NTE, modifying the free head regulatory domain, and producing the release of these heads (b). The >16-fold increase in the free head NTE straightness and rigidity upon diphosphorylation would hinder docking back of this head after swaying away as it could not recover its original interacting stereospecific disposition, hindering as well the S2 intramolecular interaction so becoming release and mobile (b, arrow). The constitutively Ser35 monophosphorylated free heads diphosphorylation induces a disorder-to-order transition which fully elongates the helix P along the helix A by establishing three salt bridges pSer35/Arg38, Arg39, and pSer45/Arg42.¹⁷ *Potentiating actuator* (yellow boxes): In contrast to the activating actuator on the free head, the potentiation actuator on the blocked head is not based on a disorder-to-order transition of the RLC NTE. The blocked head Ser45 monophosphorylation does not produce any conformational change on the NTE, except a salt bridge between pSer45 and Lys39 or pSer45 and Lys37.¹⁷ a net negative charge reduction of -2 and an ~1.8-fold increase in dynamic persistence length (ξ_d) (Table 1), suggesting that blocked head NTE monophosphorylation at Ser45 makes it more rigid, hindering the docking back of its partner free head, making it also release and mobile (d, top arrow). This in turn could weaken the blocked head RLC NTE electrostatic interaction with a loop on the motor domain of the neighbour free head, making the blocked head to sway away (c). This is functionally important since the blocked heads monophosphorylation at Ser45 by MLCK is an effective way to recruit potentiating heads (Fig. 4c). FH and BH: free and blocked heads.

References

- 1 W. Lehman and A. G. Szent-Györgyi, *J. Gen. Physiol.*, 1975, **66**, 1-30.
- 2 A. Szent-Györgyi, *Regulatory Mechanisms of Striated Muscle Contraction*, Springer Japan, 2007, **592**, 253-264.
- 3 J. T. Stull, D. K. Blumenthal and R. Cooke, *Biochem. Pharmacol.*, 1980, **29**, 2537-2543.
- 4 J. R. Sellers, *J. Biol. Chem.*, 1981, **256**, 9274-9278.
- 5 R. Craig, R. Padrón and J. Kendrick-Jones, *J. Cell. Biol.*, 1987, **105**, 1319-1327.
- 6 A. Pinto, F. Sánchez, L. Alamo and R. Padrón, *J. Struct. Biol.*, 2012, **180**, 469-478.
- 7 R. Padrón, N. Panté, H. Sosa and J. Kendrick-Jones, *J. Muscle Res. Cell Motil.*, 1991, **12**, 235-241.
- 8 C. Hidalgo, R. Craig, M. Ikebe and R. Padrón, *J. Muscle Res. Cell Motil.*, 2001, **22**, 51-59.
- 9 R. Craig and W. Lehman, *J. Mol. Biol.*, 2001, **311**, 1027-1036.
- 10 L. Alamo, W. Wriggers, A. Pinto, F. Bártoli, L. Salazar, F.-Q. Zhao, R. Craig and R. Padrón, *J. Mol. Biol.*, 2008, **384**, 780-797.
- 11 R. Brito, L. Alamo, U. Lundberg, J. R. Guerrero, A. Pinto, G. Sulbarán, M. A. Gawinowicz, R. Craig and R. Padrón, *J. Mol. Biol.*, 2011, **414**, 44-61.
- 12 G. Sulbarán, A. Biasutto, L. Alamo, C. Riggs, A. Pinto, F. Méndez, R. Craig and R. Padrón, *Biophys. J.*, 2013, **105**, 2114-2122.
- 13 W. D. Nelson, S. E. Blakely, Y. E. Nesmelov and D. D. Thomas, *Proc. Natl. Acad. Sci. U.S.A.*, 2005, **102**, 4000-4005.
- 14 L. M. Espinoza-Fonseca, D. Kast and D. D. Thomas, *Biophys. J.*, 2007, **93**, 2083-2090.
- 15 D. Kast, L. M. Espinoza-Fonseca, C. Yi and D. D. Thomas, *Proc. Natl. Acad. Sci. U.S.A.*, 2010, **107**, 8207-8212.
- 16 L. M. Espinoza-Fonseca, B. A. Colson and D. D. Thomas, *Mol. Biosyst.*, 2014, **10**, 2693-2698.
- 17 L. M. Espinoza-Fonseca, L. Alamo, A. Pinto, D. D. Thomas, and R. Padrón, 201, *Mol. Biosyst.*, 2015, (submitted).
- 18 S. Hvídt, J. D. Ferry, D. L. Roelke and M. L. Greaser, *Macromolecules*, 1983, **16**, 740-745.
- 19 X. E. Li, W. Lehman, S. Fischer and K. C. Holmes, *J. Struct. Biol.*, 2010, **170**, 307-312.
- 20 X. E. Li, W. Lehman, S. Fischer and K. C. Holmes, *J. Struct. Biol.*, 2010, **170**, 313-318.
- 21 X. E. Li, K. C. Holmes, W. Lehman, H. Jung and S. Fischer, *J. Mol. Biol.*, 2010, **395**, 327-339.
- 22 N. Guex and M. C. Peitsch, *Electrophoresis*, 1997, **18**, 2714-2723.
- 23 A. D. MacKerell, D. Bashford, M. Bellott, R. L. Dunbrack, J. D. Evanseck, M. J. Field, S. Fischer, J. Gao, H. Guo, S. Ha, D. Joseph-McCarthy, L. Kuchnir, K. Kuczera, F. T. K. Lau, C. Mattos, S. Michnick, T. Ngo, D. T. Nguyen, B. Prodhom, W. E. Reiher, B. Roux, M. Schlenkrich, J. C. Smith, R. Stote, J. Straub, M. Watanabe, J. Wiórkiewicz-Kuczera, D. Yin and M. Karplus, *J. Phys. Chem. B*, 1998, **102**, 3586-3616.
- 24 L. Kalé, R. Skeel, M. Bhandarkar, R. Brunner, A. Gursoy, N. Krawetz, J. Phillips, A. Shinozaki, K. Varadarajan and K. Schulten, *J. Comput. Phys.*, 1999, **151**, 283-312.
- 25 W. Weber, P. H. Hünenberger and J. A. McCammon, *J. Phys. Chem. B*, 2000, **104**, 3668-3675.
- 26 T. Darden, D. York and L. Pedersen, *J. Chem. Phys.*, 1993, **98**, 10089-10092.
- 27 U. Essmann, L. Perera, M. L. Berkowitz, T. Darden, H. Lee and L. G. Pedersen, *J. Chem. Phys.*, 1995, **103**, 8577-8593.
- 28 E. F. Pettersen, T. D. Goddard, C. C. Huang, G. S. Couch, D. M. Greenblatt, E. C. Meng and T. E. Ferrin, *J. Comput. Chem.*, 2004, **25**, 1605-1612.
- 29 W. Humphrey, A. Dalke and K. Schulten, *J. Mol. Graph.*, 1996, **14**, 33-38.
- 30 D. Frishman and P. Argos, *Proteins: Struct., Funct., Bioinf.*, 1995, **23**, 566-579.
- 31 E. N. Trifonov, R. K. Z. Tan and S. C. Harvey, In *DNA Bending and Curvature* (W. K. Olson, M. H. Sarma and M. Sundaralingam, eds) Adenine Press., New York, 1987, 243-253.
- 32 J. A. Schellman and S. C. Harvey, *Biophys. Chem.*, 1995, **55**, 95-114.
- 33 G. Zuccheri, A. Scipioni, V. Cavaliere, G. Gargiulo, P. De Santis and B. Samori, *Proc. Natl. Acad. Sci. U.S.A.*, 2001, **98**, 3074-3079.

- 34 J. L. Woodhead, F.-Q. Zhao, R. Craig, E. H. Egelman, L. Alamo and R. Padrón, *Nature*, 2005, **436**, 1195-1199.
- 35 H. M. Berman, T. Bhat, P. E. Bourne, Z. Feng, G. Gilliland, H. Weissig and J. Westbrook, *Nat. Struct. Biol.*, 2000, **11**, 957-959.
- 5 36 S. Sivaramakrishnan, B. J. Spink, A. Y. Sim, S. Doniach and J. A. Spudich, *Proc. Natl. Acad. Sci. U.S.A.*, 2008, **105**, 13356-13361.
- 37 H. Huxley, *Science*, 1969, **164**, 1356-1366.
- 10 38 G. Sulbarán, L. Alamo, A. Pinto, G. Marquéz, F. Méndez, R. Padrón and R. Craig, *Biophys. J.*, 2015, **106**, 159a.
- 39 L. M. Espinoza-Fonseca, D. Kast and D. D. Thomas, *J. Am. Chem. Soc.*, 2008, **130**, 12208-12209.
- 40 H. S. Jung, N. Billington, K. Thirumurugan, B. Salzameda, C. R. Cremo, J. M. Chalovich, P. D. Chantler and P. J. Knight, *J. Mol. Biol.*, 2011, **408**, 863-878.
- 15
- 41 K. A. Taylor, M. Feig, C. L. Brooks, P. M. Fagnant, S. Lowey and K. M. Trybus, *J. Struct. Biol.*, 2014, **185**, 375-382.
- 20 42 P. R. Steinmetz, J. E. Kraus, C. Larroux, Jö. U., Amon-Hassenzahl, A., Houliston, E., Wörheide, G., Nickel, M., Degnan, B. M. and Technau, U. Hammel, *Nature*, 2012, **487**, 231-234.
- 43 K. Seipel and V. Schmid, *Dev. Biol.*, 2005, **282**, 14-26.
- 25 44 P. Schuchert, S. Reber-Müller and V. Schmid, *Differentiation*, 1993, **54**, 11-18.
- 45 T. Wendt, D. Taylor, K. M. Trybus and K. Taylor, *Proc. Natl. Acad. Sci. U.S.A.*, 2001, **98**, 4361-4366.
- 30

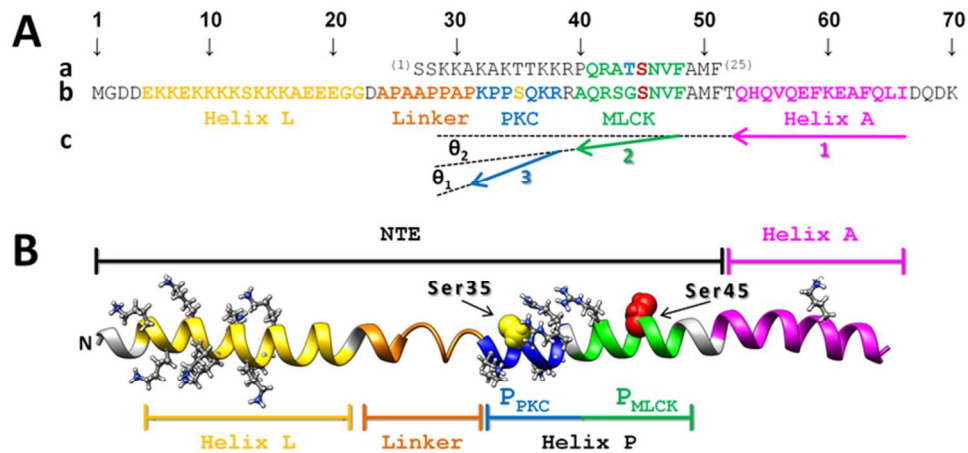


Fig. 1 The NTEs of the smooth and tarantula myosin RLCs. (A) Sequence alignment of the NTEs of chicken smooth (a) and tarantula striated (b) muscles. Phosphorylatable serines are in yellow (Ser35) and red (Ser45). Helix L (yellow), coil Pro/Ala linker (orange), helix P formed by PKC (blue) and MLCK (green) target consensus sequences, adjacent to the EF helix A (purple, Gln53-Ile66).¹⁰ (c) Vectors and angles as defined for the flexural rigidity analysis (see Methods). (B) Straightened tarantula RLC fragment used as the starting structure for MD simulations and flexural rigidity analysis. The 52-aa NTE (formed by helix L, linker and helix P) is adjacent to the RLC helix A (purple). The helix L has 9 positively charged lysines, and is connected by a flexible linker to the helix P, with includes the PKC (P_{PKC} , blue) and MLCK (P_{MLCK} , green) consensus sequences with their phosphorylatable Ser35 and Ser45.

70x35mm (300 x 300 DPI)

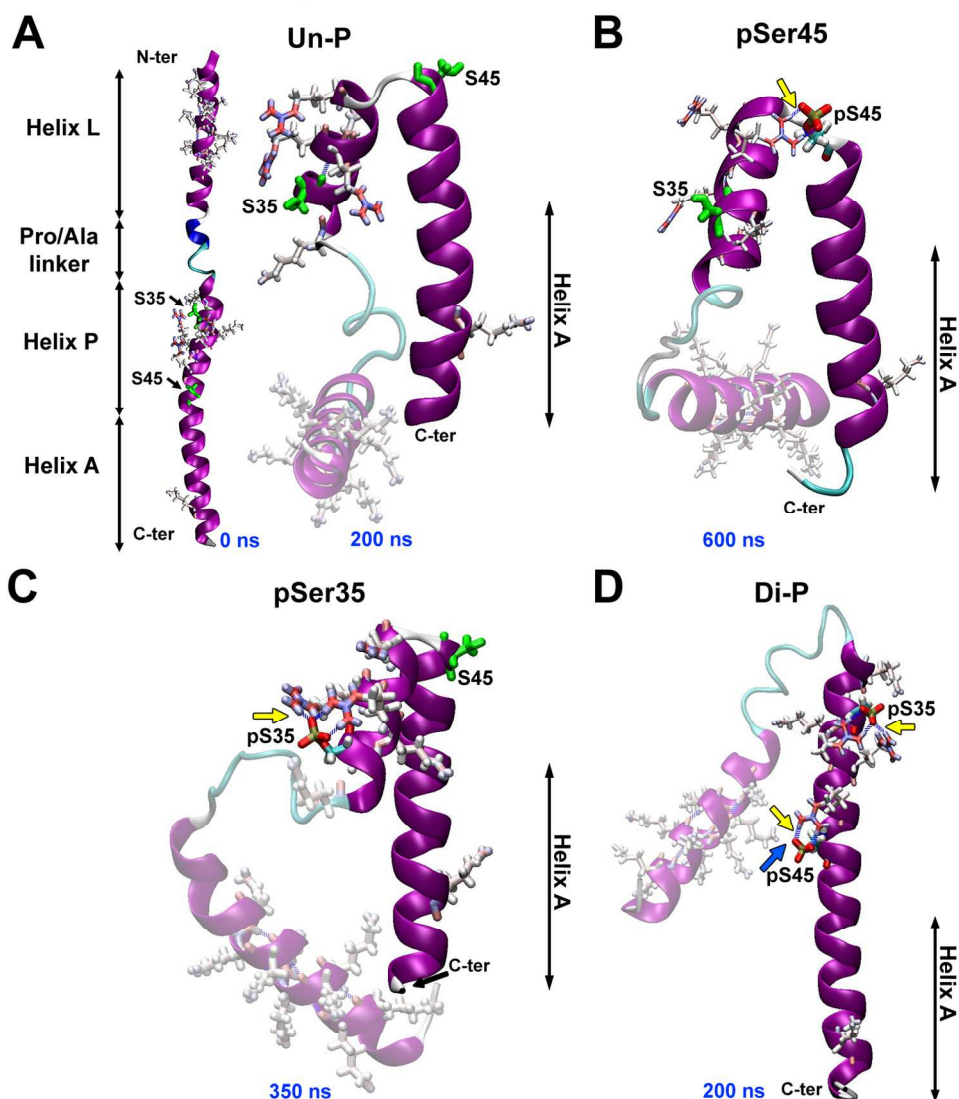


Fig. 2 Snapshots showing key structural features of trajectories. The starting structure was assumed to be a straight α -helix. This peptide was equilibrated for the un-P (shown on the left part of A), pSer45, pSer35 and di-P MD simulations. Final simulation states of the stabilized structures are shown on A-D. Helix P bends bent over helix A in A-C but stays straightened on D. There is a linker extension at Pro31-Lys32 becomes coil/turn in A and C but not in B and D. Helix P is always bend at Ser45 except in D, where helices P and A remain straight. No salt bridges are established in un-P state A. Salt bridges (yellow arrows) are established for the mono-P states: pSer35/Arg38,Arg39 in C or pSer45/Arg39 in B; and salt bridges pSer35/Arg38,Arg39, and pSer45/Arg42 in D. Helix L (shadowed) moves freely around the flexible linker in all conditions, interacting eventually with helix-A in A-C, but in di-P (D) inter-helix pSer45/Lys15 salt bridge between helix L and A is established (blue arrow).

140x160mm (300 x 300 DPI)

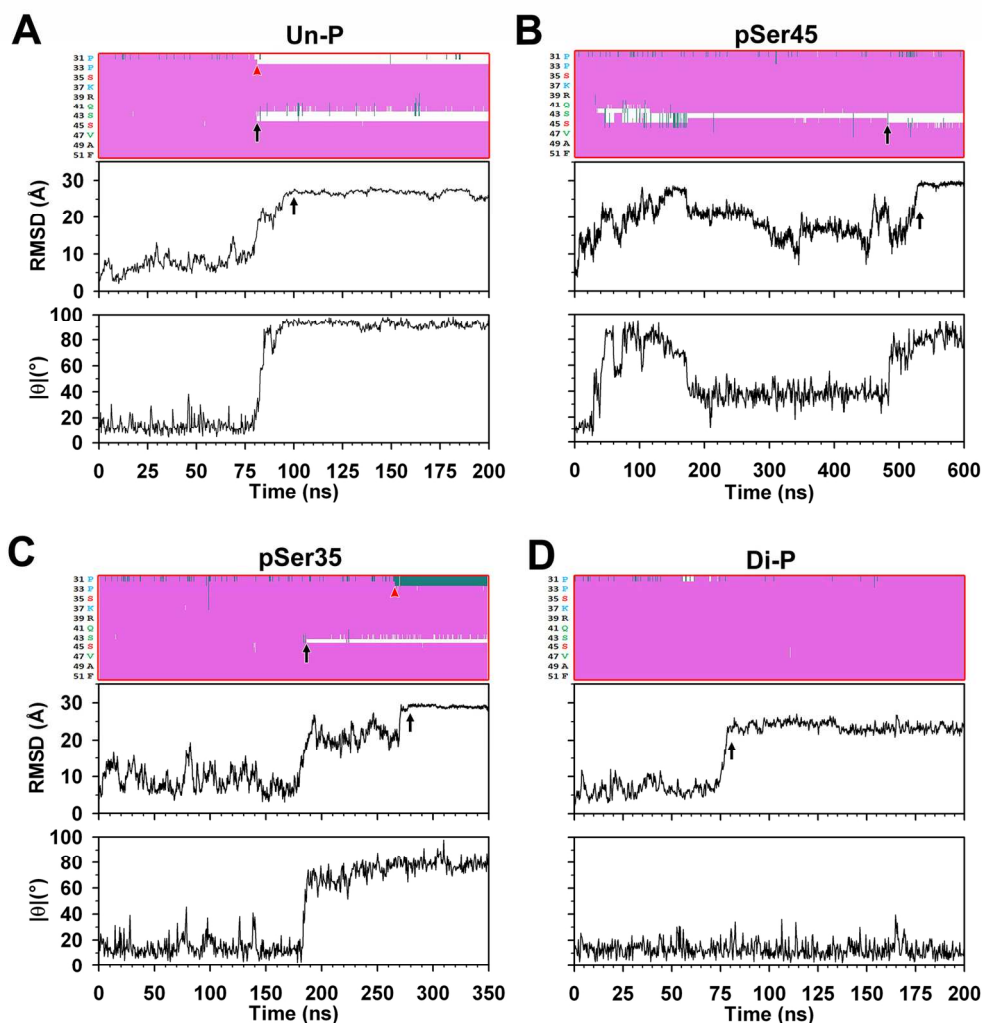


Fig. 3 *Top panels:* Evolution of secondary structure of NTE helix P along their trajectories: un-P (A), Ser45 (B) or Ser35 (C) mono-P, and di-P (D). Snapshots illustrating the final key structural features are shown in Fig. 2. Helix to coil/turns: at Pro31-Lys32 (A,C) (red arrowheads). HCH: at Ser43-Gly44 (A, B) and Gly44 (C) (black arrows). Vertical axis: one-letter code aa number. Secondary structure key colours: α -helix (pink), turn (cyan), coil (white). *Centre panel:* root mean square deviation (RMSD) of the NTE peptides trajectories of each phosphorylated state shown in Fig. 2. Arrows show that peptides stabilized after 100 (A), 530 (B), 300 (C) and 80 (D) ns. *Bottom panel:* Persistence length analysis ($|\theta|$ vs. time) of the NTEs. The angle $|\theta|$ captures the bending of the α -helix of the three vectors regions (Fig. 1Ac). The angle $|\theta|$ changed to $\sim 90^\circ$ for the un-P (A), to $\sim 80^\circ$ for Ser45 (B) or Ser35 (C) mono-P cases, and does not changed much ($\sim 10^\circ$) for the Di-P state (D). The result in (D) shows an important increase of straightening and rigidification (Table 1) only induced by diphosphorylation.

149x160mm (300 x 300 DPI)

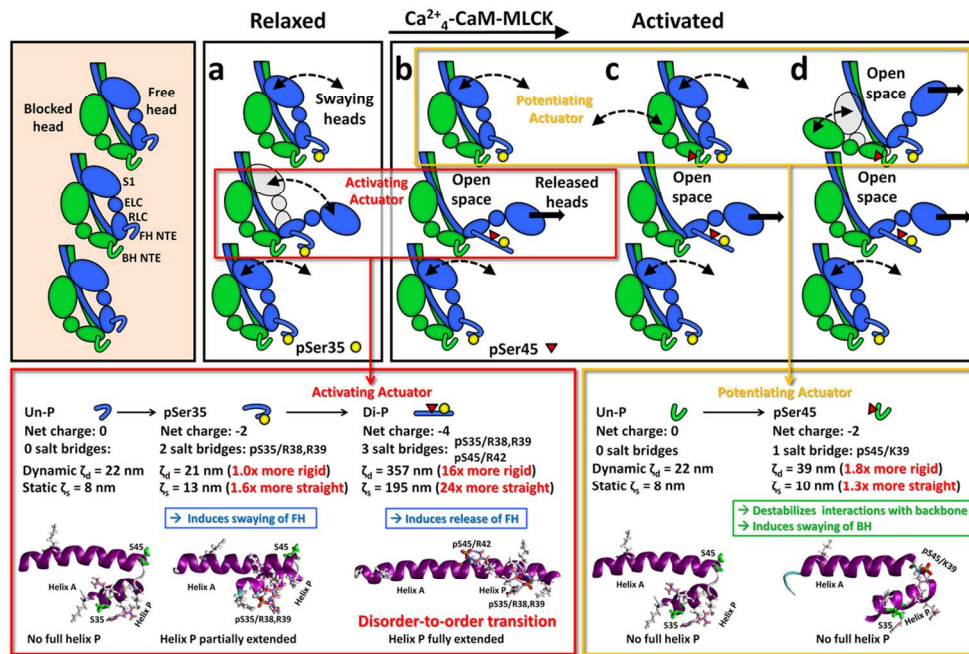


Fig. 4 The *cooperative phosphorylation-controlled mechanism* for recruiting active heads in tarantula thick filament activation.^{11,12,17} The three myosin interacting-heads motifs on the left are shown along one thick filament helix with their entire RLC NTEs unphosphorylated (bare zone at the top). This mechanism shows how the Ser45 phosphorylation of the constitutive Ser35 monophosphorylated swaying free head NTE (b, centre IHM) hinders its docking back making it release and mobile (b, arrow). Two *actuators* (red and yellow boxes) control the sequential release of myosin heads on tarantula thick filament activation.¹⁷ *Activating actuator* (red boxes): according to our MD simulations the activating actuator is based on a disorder-to-order transition of the RLC NTE, which induces its elongation in accordance with the increase of the static and dynamic persistence length ξ_s and ξ_d . This implies a substantial straightening and rigidification of the diphosphorylated NTE, modifying the free head regulatory domain, and producing the release of these heads (b). The >16-fold increase in the free head NTE straightness and rigidity upon diphosphorylation would hinder docking back of this head after swaying away as it could not recover its original interacting stereospecific disposition, hindering as well the S2 intramolecular interaction so becoming release and mobile (b, arrow). The constitutively Ser35 monophosphorylated free heads diphosphorylation induces a disorder-to-order transition which fully elongates the helix P along the helix A by establishing three salt bridges pSer35/Arg38,Arg39, and pSer45/Arg42.¹⁷ *Potentiating actuator* (yellow boxes): In contrast to the activating actuator on the free head, the potentiation actuator on the blocked head is not based on a disorder-to-order transition of the RLC NTE. The blocked head Ser45 monophosphorylation does not produce any conformational change on the NTE, except a salt bridge between pSer45 and Lys39 or pSer45 and Lys37, a net negative charge reduction of -2 and an ~1.8-fold increase in dynamic persistence length (ξ_d) (Table 1), suggesting that blocked head NTE monophosphorylation at Ser45 makes it more rigid, hindering the docking back of its partner free head, making it also release and mobile (d, top arrow). This in turn could weaken the blocked head RLC NTE electrostatic interaction with a loop on the motor domain of the neighbour free head, making the blocked head to sway away (c). This is functionally important since the blocked heads monophosphorylation at Ser45 by MLCK is an effective way to recruit potentiating heads (Fig. 4c). FH and BH: free and blocked heads.

108x72mm (300 x 300 DPI)